PROCEEDINGS, TOUGH Symposium 2003
Lawrence Berkeley National Laboratory, Berkeley, California, May 12–14, 2003

STRATEGIES FOR GAS PRODUCTION FROM HYDRATE ACCUMULATIONS UNDER VARIOUS GEOLOGICAL AND RESERVOIR CONDITIONS

George J. Moridis and Timothy S. Collett

Lawrence Berkeley National Laboratory, 1 Cyclotron Rd., ESD, MS90-1116, Berkeley, CA 94720, U.S.A.
U.S. Geological Survey, Denver Federal Center, Box 2504 MS939, Denver, CO 80225, U.S.A.
e-mail: GJMoridis@lbl.gov, TSCollett@usgs.gov

ABSTRACT

In this paper we classify hydrate deposits in three classes according to their geologic and reservoir conditions, and discuss the corresponding production strategies. Simple depressurization appears promising in Class 1 hydrates, but its appeal decreases in Class 2 and Class 3 hydrates. The most promising production strategy in Class 2 hydrates involves combinations of depressurization and thermal stimulation, and is clearly enhanced by multi-well production-injection systems. The effectiveness of simple depressurization in Class 3 hydrates is limited, and thermal stimulation (alone or in combination with depressurization) through single well systems seems to be the strategy of choice in such deposits.

INTRODUCTION

Gas hydrates are solid crystalline compounds in which gas molecules are encaged inside the lattices of ice crystals. Vast amounts of hydrocarbons are trapped in hydrate deposits (Sloan, 1998). Such deposits exist under favorable thermodynamic conditions, which occur in two distinctly different types of geologic formation where the necessary low temperatures and high pressures exist: in the permafrost and in deep ocean sediments.

Current estimates of the worldwide quantity of hydrocarbon gas hydrates range between 10^{15} to 10^{18} m^3. Even the most conservative estimates of the total quantity of gas in hydrates may surpass by a factor of two the energy content of the total fuel fossil reserves recoverable by conventional methods (Sloan, 1998). The magnitude of this resource could make hydrate reservoirs a substantial future energy resource. Although the current energy economics cannot support gas production from hydrate accumulations, their potential clearly demands further evaluation.

THE NUMERICAL MODEL

The numerical studies of gas production in this paper were conducted using the TOUGH2 general-purpose simulator (Pruess et al., 1999) for multi-component, multiphase fluid and heat flow and transport in the subsurface with the EOSHYDR2 module (Moridis et al., 1998; Moridis, 2002a). By solving the coupled equations of mass and heat balance, EOSHYDR2 models the behavior of methane-bearing binary hydrates that are formed or dissociate in porous media according to the general reaction equation:

$$\chi_m[CH_4 \cdot n_m H_2O] \cdot \chi_G[G \cdot n_G H_2O] = \chi_m CH_4 + \chi_G G + (n_m + n_G) H_2O$$

where G is the second hydrate-forming gas, n is the hydration number, χ is the mole fraction in the binary hydrate, and the subscripts m and G denote the methane and the second gas, respectively. Obviously, $\chi_m+\chi_G = 1$. The gaseous component G can be one of CO_2, H_2S, N_2, or another gaseous alkane $C_\square H_{\square\square\square}$ ($\square$ = 2, 3, 4). Although χ_m often exceeds 0.95 in natural hydrates, the second gaseous component G cannot be ignored because it can have a profound effect on the hydration pressure and temperature even when χ_G = 0.01 (Sloan, 1998). EOSHYDR2 can describe the non-isothermal hydrate formation and/or dissociation, gas release, phase behavior, and fluid and heat flow under conditions typical of either type of methane-bearing binary hydrate deposits.

EOSHYDR2 includes both an equilibrium and a kinetic model of gas hydrate formation and dissociation. The model accounts for heat and up to eight mass components: hydrate, water, native methane and methane from the hydrate dissociation, a second hydrate-forming gas (native and from dissociation), salt, and a water-soluble inhibitor (such as an alcohol). The mass components are distributed among four phases, i.e., a gas phase, a liquid phase, and two solid immobile phases: an ice phase and the hydrate phase. The thermophysical properties of the various mass components can be described at temperatures as low as –110 ^{o}C. Dissociation, phase changes and the corresponding thermal effects are accounted for, as are the effects of salt and hydrate inhibitors. The model can describe gas hydrate dissociation involving any combination of the possible dissociation mechanisms (i.e., depressurization, thermal stimulation, as well as inhibitor and salting-out effects).

CLASSIFICATION OF NATURAL HYDRATE ACCUMULATIONS

In terms of characteristics and behavior (which, in turn, dictate production strategies), hydrate accumulations can be divided into three main classes. Class 1 accumulations comprise two zones: the hydrate interval (often exhibiting a very low effective permeability because of the presence of large hydrate saturations in the pore space), and an underlying two-phase fluid zone with free (mobile) gas. In this class, the bottom of the hydrate stability zone usually coincides with the bottom of the hydrate interval. In terms of gas production, this is the most desirable class for exploitation because of the hydrate thermodynamic proximity to the hydration equilibrium (necessitating only small changes in pressure and temperature to induce dissociation).

Class 2 deposits feature two zones: a hydrate-bearing interval, overlying a mobile water zone with no free gas (e.g., an aquifer). Class 3 accumulations include a single zone, the hydrate interval, and are characterized by the absence of an underlying zone of mobile fluids. In Classes 2 and 3, the entire hydrate interval may be well within the hydrate stability zone, i.e., the bottom of the hydrate interval does not mark the bottom of the hydrate stability zone. The desirability of Class 2 and 3 accumulations as gas production targets is less well defined than for Class 1 deposits, and can be a complex function of several issues, including thermodynamic proximity to hydration equilibrium, initial conditions, environmental concerns and economic considerations.

In the ensuing discussion we focus on permafrost hydrate deposits because of the availability of field data. The results generally apply to ocean deposits, although boundary conditions can play a more important role in such accumulations.

Figure 1. Gas production from a Class 1 hydrate accumulation in the North Slope, Alaska.

GAS PRODUCTION FROM CLASS 1 HYDRATE ACCUMULATIONS

The schematic in Figure 1 shows gas production from a Class 1 hydrate accumulation in the North Slope of Alaska. The initial conditions in the hydrate zone and in the underlying free gas zone, as well as all pertinent hydraulic and operational parameters, are listed on Figure 1. Gas is produced from five identical wells producing from the free gas zone at a cumulative rate of $Q = 4.2475 \times 10^6$ standard m^3/day (1.5×10^8 ft^3/day). This production scenario leads to depressurization-induced hydrate dissociation.

The grid used in this 3-D simulation involved about 60,000 elements, and described only half the system depicted in Figure 1 because of symmetry. Only pure CH_4-hydrate was considered. Five components were considered in the simulations: CH_4-hydrate, H_2O, CH_4 from the free zone, CH_4 from hydrate dissociation (thus enabling tracking directly and separately the contributions of the two CH_4 sources to the production stream), and heat. The most challenging part of the simulation involved the determination of the areally-variable appropriate initial conditions, i.e., of the initial distributions of pressure, temperature, and saturations (gas, water and hydrate) that would result in (a) physically meaningful geothermal gradients, (b) a hydraulic-hydrostatic equilibrium, and (c) hydration equilibrium that would lead to the appearance of the numerically predicted hydrate interface at an elevation matching the known field location.

Figure 2 shows the cumulative volumes of hydrate-originating CH_4 released during the depressurization-induced dissociation (both equilibrium and kinetic). For comparison, the cumulative gas volume produced from the system over the duration of the study is also shown. A comparison of these curves provides a measure of the level of replacement of gas from the free-gas zone by CH_4 released during dissociation.

The results in Figure 2 indicate that, assuming an equilibrium process, dissociation replaces a very large portion of the CH_4 produced from the free-gas zone. The replenished gas portion can be as high as 90%, and declines at later times, but is well above the 50% level at the end of the four-year study period. The volume of gas released under a kinetic dissociation regime is substantially smaller.

The corresponding effects on the pressure evolution in the free-gas zone are shown in Figure 3. Under equilibrium dissociation, the pressure decline is much milder than that for kinetic dissociation.

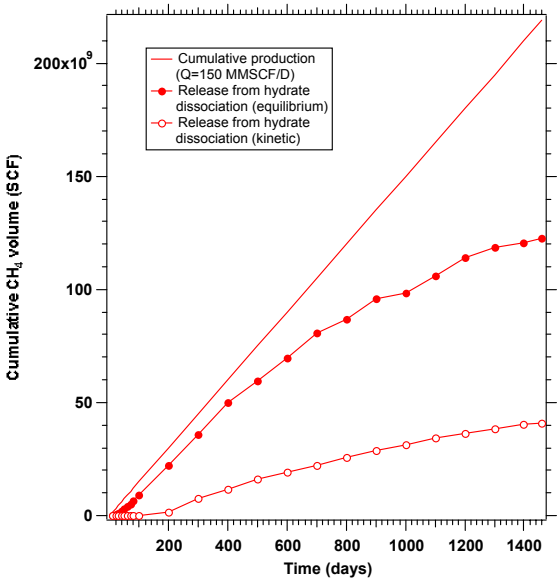

Figure 2. Cumulative release of CH_4 from hydrate dissociation during gas production from the Class 1 hydrate in Figure 1.

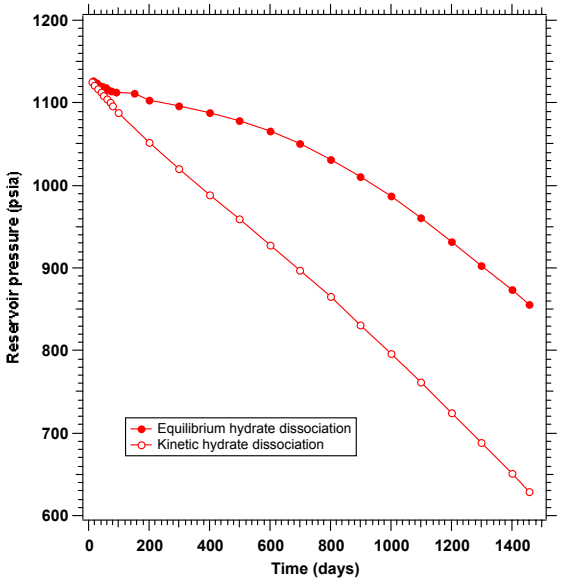

Figure 3. Pressure evolution during gas production from the hydrate deposit in Figure 1.

This is because, under equilibrium dissociation, the free gas zone is replenished by large CH_4 releases from the dissociating hydrate. Under kinetic dissociation, the CH_4 releases are much lower, resulting in a steeper pressure decline.

The results are elucidated in Figure 4, which shows the evolution over time of the rate of CH_4 release under equilibrium-dissociation conditions. The rate increases initially, because the pressure drop in the free gas zone (caused by the gas production) increases with time, leading to larger pressure differentials and, consequently, larger driving forces for depressurization-induced dissociation and larger volumes of released gas.

However, the rate begins to decline after a maximum is reached at about t = 220 days. This occurs when the effect of increasing depressurization is overcome by the counter-acting progressive cooling of the hydrate (due to the strongly endothermic nature of dissociation), which makes dissociation increasingly difficult.

In Figure 5, the CH_4 release rates under kinetic dissociation show a different behavior in terms of both the pattern and the magnitude of the rate evolution over time. The initial release rate is very small (because the large permeability of the formation results in a very mild and uniformly distributed pressure decline), but begins increasing rapidly as the pressure drop increases while the temperature is not strongly affected. This is followed by a period of roughly stable release rate (from t=200 to t = 600 days), indicating parity between the effects of depressurization and cooling on dissociation. After this period, the release rate begins to decline as the effects of depressurization are overwhelmed by the adverse consequences of hydrate cooling.

Note that this is a particularly appealing specimen of a Class 1 hydrate deposit, characterized by the confluence of all possible conditions favorable to enhanced gas production from hydrate dissociation. This accumulation is endowed by a thick free-gas zone (91.5 m = 300 ft), a thick hydrate zone (about 183 m = 600 ft), a very large interface area of the hydrate with the free gas, and a large intrinsic permeability (10^{-12} m^2 = 1 darcy). The bottom of the hydrate zone is at equilibrium, requiring a very small perturbation of pressure or temperature for gas dissociation to begin.

The large intrinsic permeability indicates low capillary pressures, and, coupled with the thick free gas-zone, leads to low water saturations in the vadose zone and rapid drainage of the very large amounts of water released during dissociation. This combination of factors prevents the build-up of water saturation in the vicinity of the dissociating hydrate, and alleviates the potential problem of impeded gas flows due to the resulting adverse relative permeability conditions. The dip of the system allows concentration of the draining water near the lowest point of the formation, thus localizing water storage and limiting its potentially adverse effects on dissociation.

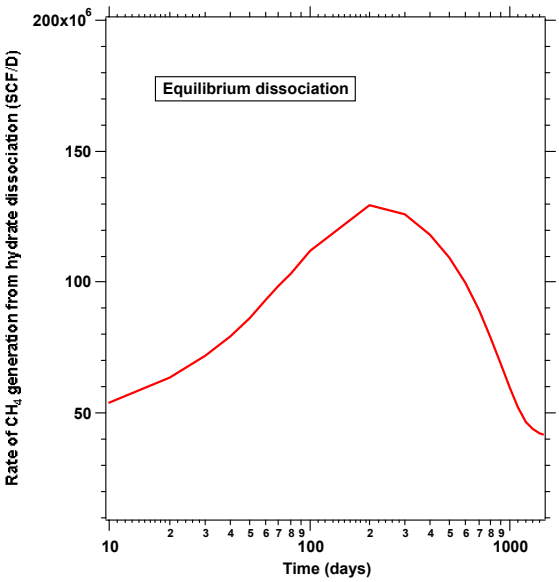

Figure 4. Release rate of CH_4 from the equilibrium dissociation of the hydrate deposit in Figure 1.

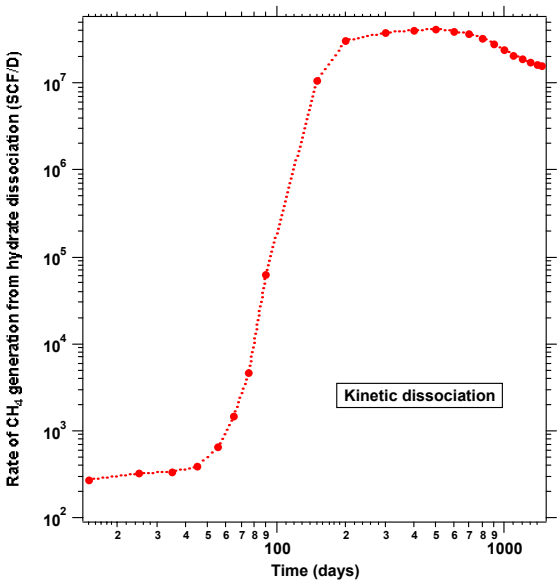

Figure 5. Release rate of CH_4 from the kinetic dissociation of the hydrate deposit in Figure 1.

The large intrinsic permeability results in pressure declines that are mild and nearly uniform in the reservoir. Exposure of the very large hydrate-gas interface to these uniform pressure drops results in dissociation from practically the entire interface. Additionally, the mild pressure drops allow cooling to be slower and distributed over the whole interface, thus allowing more effective heat transfer from the surroundings and higher overall temperatures. Such mild processes are far better in allowing the slow process of heat conduction to supply the heat necessary for dissociation than steeper pressure gradients. Such steeper conditions may lead to an initial burst of gas release, but this is localized and self-limiting because the resulting rapid cooling overwhelms the slow mechanism of heat conduction (the only energy source under pure depressurization) and leads to increasingly slower dissociation.

GAS PRODUCTION FROM CLASS 2 HYDRATE ACCUMULATIONS

An initial review of Class 2 hydrate accumulations indicates significant positive features. Because of the near-incompressibility of water, depressurization appears to be more effective than in Class 1 hydrates because the pressure disturbance is stronger and is usually sensed by a large area of the hydrate-water interface. Additionally, the presence of water with its relatively heat capacity provides an additional significant heat reservoir to supply the needs of the endothermic dissociation reaction.

However, upon further study, Class 2 hydrates reveal serious shortcomings. Despite the favorable depressurization regime, gas production is hampered by the adverse relative permeability conditions of emergence and maintenance of a gas phase in a previously fully-saturated water zone. In single well configurations, depressurization-induced gas production is accompanied by very significant water production that represents up to 98% of the total produced mass (Moridis et al., 2002). Disposing of such large volumes of water in environmentally sensitive areas (such as the North Slope) may be fraught with complications, in addition to the economic considerations related to the pumping out and disposing of such large volumes of water.

Moridis (2002b) highlighted the limited potential of single-well systems, and proposed an approach involving multi-well (five-spot) systems with net zero water withdrawals that could maximize production from Class 2 hydrate accumulations. Reservoir fluids (i.e., H_2O and gas from dissociation) were produced from the four production wells at rates determined by the relative permeabilities, and hot water was injected into the center-well at a rate equal to the production rate after heating it with a portion of the produced gas. The obvious advantage of this scheme is that it combines the two most important mechanisms of hydrate dissociation, i.e., depressurization at the production well, and thermal stimulation at the injection well. By appropriate placement of the injection and production intervals, mixing of the injected hot water with the colder native reservoir water was minimized, while

maximizing the thermal advantages of buoyancy that tended to concentrate the warmer water immediately below the targeted hydrate interface.

In these simulations, data from the Mallik accumulation were used (Dallimore et al., 1999). The hydrate layer is 16 m thick, and is underlain by 2-m-thick water-saturated layer. The hydrate and water saturations in the hydrate interval are S_H = 0.8 and S_w = 0.2, respectively. At the bottom of the hydrate interval, the pressure P = 9 MPa and the temperature was T = 7.5 °C. Because of symmetry, only a quarter of the domain was simulated using a 3-D Cartesian system. The side of the simulated quadrant was 30 m. The domain was discretized in 46x46x33 unequally spaced subdivisions in (x,y,z), resulting in almost 70,000 gridblocks. Four equations (one for each components, i.e., CH_4 from dissociation, H_2O, hydrate, salt) and one heat balance equation were considered in each gridblock, leading to a system of about 350,000 simultaneous equations. In the base case, the initial water injection and production rate was Q = 2400 kg/day, and the injection temperature was T_w = 50 °C.

There are two possible sources of the evolving gas: CH_4 originating from the depressurization-induced dissociation of hydrates in the vicinity of the production well (hereafter referred to as D-gas), and CH_4 from the thermal dissociation of hydrates in the vicinity of the hot-water injection well (hereafter referred to as T-gas). Figure 6 (Moridis, 2002b) shows the cumulative, D-gas and T-gas releases in Zone A over a 90-day period. As expected, D-gas emerges earlier than T-gas because of the speed of propagation of the pressure wave and the significant thermal inertia of hydrate-impregnated media (hydrate being a relative thermal insulator). However, the pressure drop due to fluid withdrawal is relatively small. Thus, driving depressurization-induced hydrate dissociation is limited, and is further hampered by a temperature decline in the vicinity of the production well (steeper before the hot water front arrives at the production well). This is caused by the endothermic nature of the hydrate dissociation reaction, and leads to an increase in the hydrate dissociation pressure, thus making hydrate dissociation progressively more difficult. The result is that the contribution of T-gas overtakes that of D-gas at an early stage.

These observations are confirmed by the hydrate saturation distribution in Figure 7, which shows the decay of hydrate near the hot water injection well. Note the sharp hydrate interface (demonstrated by the bunching of the saturation contour lines). This was expected because of the low relative permeability to

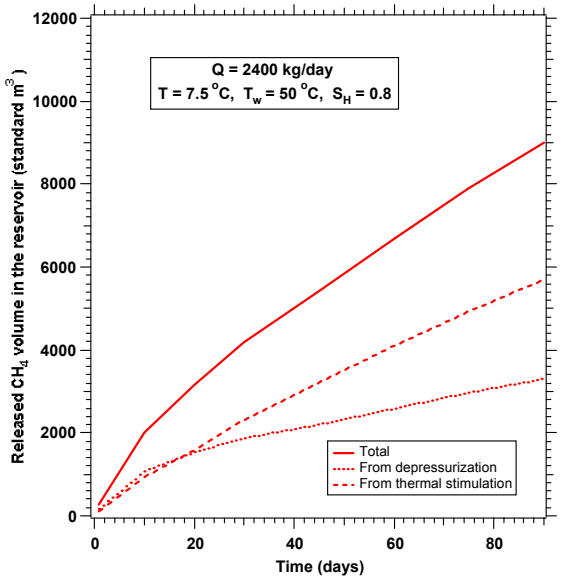

Figure 6. CH_4 volume released in the reservoir - Class 2 hydrate deposit problem (Moridis, 2002b).

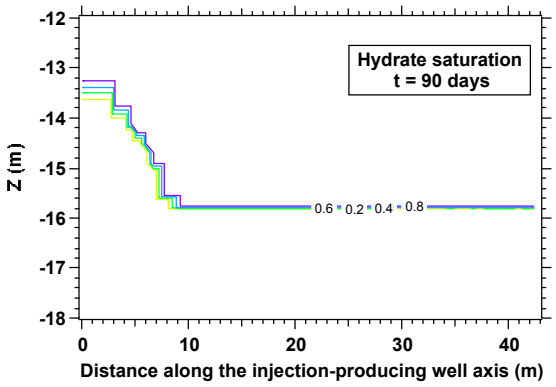

Figure 7. Hydrate saturation distribution on the injection/production plane at t=90 days- Class 2 hydrate deposit problem (Moridis, 2002b).

water (due to high initial S_H), leading to limited advection-driven heating and the dominance of conduction (a slow process).

The cumulative gas production from the production well (and the corresponding mass fraction of the gas in the production stream) appear in Figure 8. Differences from the results in Figure 6 are due to gas storage in the reservoir after dissociation. Comparison of Figures 8 and 6 indicates that the gas production and D-gas release are about equal at early times, but they begin to deviate as T-gas begins arriving at the production well. The arrival of T-gas

is marked by a change in the slope of the cumulative gas production curve. An important observation is that the produced gas represents a small fraction of the total produced mass (the rest being water), and does not exceed the 6% level during the 90-day simulation period. The gas mass fraction declines from an initial high, and then appears to stabilize at a level close to 2%. The possibility of this level rising after a longer injection-production period cannot be dismissed (as the expanding gas front from thermal dissociation reaches the production well), especially because the curve in Figure 8 shows faint signs of an upward trend. Unfortunately, the long execution times of this problem did not permit continuation of the study beyond the 90-day period.

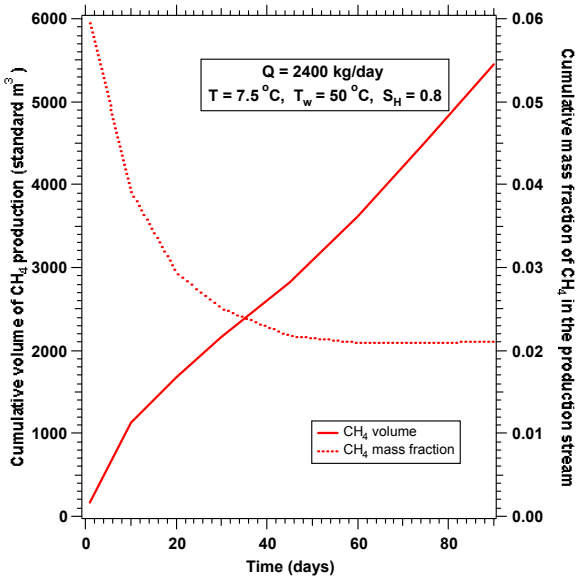

Figure 8. Cumulative CH_4 volume at the production well - Class 2 hydrate deposit problem (Moridis, 2002b).

GAS PRODUCTION FROM CLASS 3 HYDRATE ACCUMULATIONS

Class 3 hydrate accumulations do not appear to be obvious candidates for depressurization-induced dissociation. This is because desirable Class 3 hydrate deposits have a high hydrate concentration, which in turns reduces the effective permeability of reservoir fluids and makes flow through the hydrate difficult (and practically impossible if the intrinsic permeability of the medium is low). This limits the reach of depressurization to a narrow zone in the vicinity of the low-pressure (e.g., the depressurization well). The problem is compounded by the lack of permeable zones in direct contact with the hydrate interval, such as these in Class 1 and Class 2 hydrates. Thus, depressurization may be an option only if the hydrate saturation is low (reducing their value as a production target) and the intrinsic permeability is high. Because of the adverse permeability conditions, thermal stimulation appears promising in Class 3 hydrates, and may be the only production option.

The Class 3 hydrate deposit investigated here is located in the Eileen area, North Slope, Alaska, and corresponds to the C1 unit in the Northwest Eileen State-2 well (Collett, 1999). The hydrate layer is 17.2 m thick, and is assumed to be 100% CH_4-hydrate. The hydrate and water saturations in the hydrate interval are S_H = 0.71 and S_w = 0.29, respectively. At the bottom of the hydrate interval, the pressure P = 7.2426 MPa and the temperature was T = 9 °C.

A 2-D cylindrical grid was used to describe this single-well system. The domain was subdivided in 200x200 equally spaced subdivisions in (x, z), resulting in 40,000 gridblocks. Four equations (i.e., components) were considered (CH_4 from dissociation, H_2O, hydrate, and heat) in each gridblock, leading to a system of about 160,000 simultaneous equations. The well was completed in the entire hydrate interval, and thermal dissociation was induced by circulating water at a temperature T_w = 50 °C in the well.

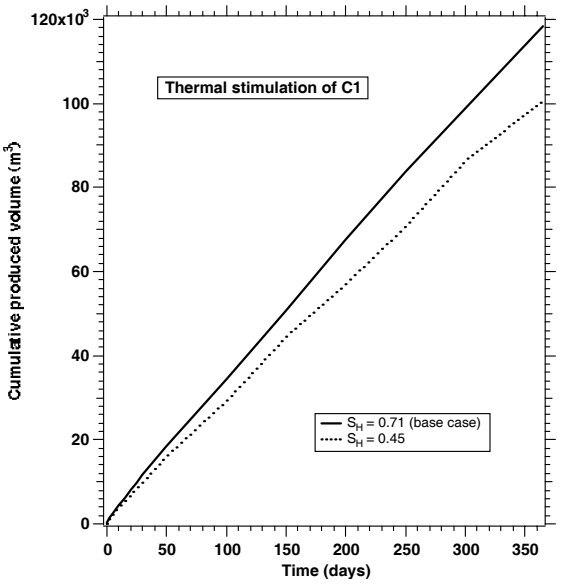

Figure 9. Gas production from the Class 3 hydrate deposit in Unit C1 of the Northwest Eileen State-2 Well, North Slope, Alaska.

The cumulative gas production is shown in Figure 9. For comparison, the cumulative gas volume for an initial S_H = 0.45 is included in the same figure, and

conforms to expectations of lower releases because of less hydrate in the pore space. When the initial temperature is assumed to be only 7 ^{o}C (only 2 ^{o}C cooler), the cumulative gas production is reduced by a factor larger than 3 (Figure 10). This is caused by the very large amounts of heat that are needed to raise the temperature of the hydrate (a thermal insulator) and of the medium to the dissociation level, reducing the heat available for dissociation.

When heat is added directly at the well bore (i.e., through electrical heating) at a rate of 6KW (roughly that at the beginning of circulation of the T_w = 50 ^{o}C water in the well), cumulative gas production increases (Figure 10) because the heat addition is unaffected by the decreasing thermal gradient between the circulating water and the formation (a situation that limits the effectiveness of thermal dissociation through hot water circulation).

The effect of operating conditions at the production well can be dramatic, as Figure 11 indicates. When the well is kept at near atmospheric pressure (by rapid removal of water in the wellbore) and electrical heat is added at the rate of 6KW, the cumulative gas production registers a spectacular increase, and exceeds that for the base case of hot water circulation (corresponding to hydrostatic pressure at the well) by a factor of about 50. The reason for this dramatic increase is the fact that this configuration allows a combination of both depressurization and thermal stimulation (i.e., the two most important dissociation mechanisms).

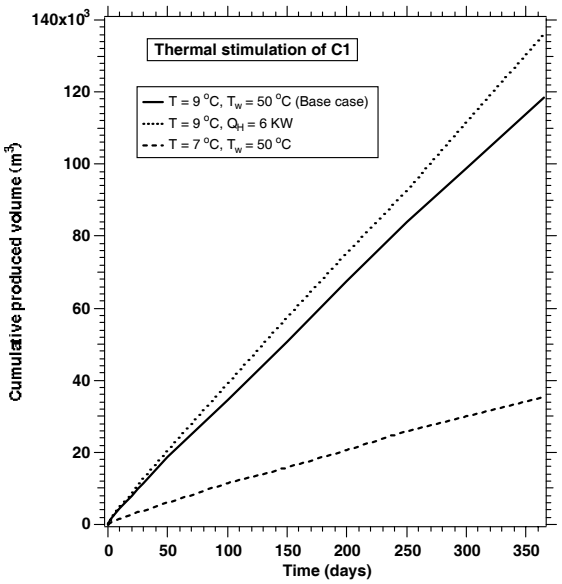

Figure 10. Effect of hydrate temperature and heat addition method on gas production from the Class 3 hydrate deposit in Unit C1 of the Northwest Eileen State-2 Well, North Slope, Alaska.

SUMMARY AND DISCUSSION

The objective of this study is the analysis of appropriate strategies for gas production from a wide range of natural hydrate accumulations. These strategies involve the two main hydrate dissociation mechanisms (depressurization and thermal stimulation) either individually or in combination. Selection of the appropriate strategy is strongly influenced by the geological setting and the conditions prevailing in the hydrate accumulation.

The TOUGH2 general-purpose simulator with the EOSHYDR2 module was used for the analysis. EOSHYDR2 models the non-isothermal gas release, phase behavior and flow in binary hydrate-bearing porous and fractured media (involving methane and another hydrate-forming gas) by solving the coupled equations of mass and heat balance, and can describe any combination of mechanisms of hydrate dissociation.

In terms of production strategy and behavior, hydrate accumulations are divided into three main classes. In Class 1 the permeable formation includes two zones: the hydrate interval and an underlying two-phase fluid zone with free (mobile) gas. In this class, the bottom of the hydrate stability zone occurs above the bottom of the permeable formation. Class 2 features a hydrate-bearing interval overlying a mobile water zone (e.g., an aquifer). Class 3 is characterized by the absence of a hydrate-free zone, and the permeable formation is thus composed of a single zone, the hydrate interval. In Classes 2 and 3, the entire hydrate interval may be well within the hydrate stability zone (i.e., the bottom of the hydrate interval does not necessarily indicate hydrate equilibrium).

We study gas production from several accumulations that span the three hydrate classes. The numerical simulations indicate that, in general, the appeal of depressurization decreases from Class 1 to Class 3, while that of thermal stimulation increases. Thus, simple depressurization appears to enjoy an advantage over other production strategies in Class 1 hydrate deposits. The most promising production strategy in Class 2 hydrates involves combinations of depressurization and thermal stimulation, and is enhanced by multi-well production-injection systems, e.g., a five-spot configuration.

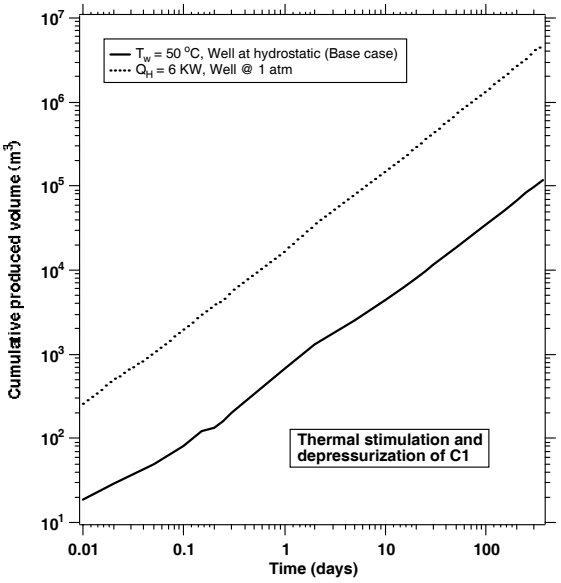

Figure 11. Effect combined thermal stimulation and depressurization on gas production from the Class 3 hydrate deposit in Unit C1 of the Northwest Eileen State-2 Well, North Slope, Alaska.

Because of the very low permeability of hydrate-bearing sediments, the effectiveness of depressurization in Class 3 hydrates is limited, and thermal stimulation through single well systems seems to be the strategy of choice in such deposits (and especially so in high hydrate saturation regimes).

These observations should only be viewed as general principles because the significant variability within each class, the case sensitivity and the insufficient body of prior experience on hydrates do not allow the outright dismissal of any production strategy in any class. The sensitivity of production to important parameters and conditions is investigated, and the limitations of the various production strategies are discussed.

ACKNOWLEDGMENT

This work was supported by the Assistant Secretary for Fossil Energy, Office of Natural Gas and Petroleum Technology, through the National Energy Technology Laboratory, under the U.S. Department of Energy, Contract No. DE-AC03-76SF00098. Thanks are extended to Scott Digert and Robert Hunter for provided important data for the Class 1 hydrate deposit discussed in the paper. The author is indebted to Yonkoo Seol and John Apps for their insightful review comments.

REFERENCES

Collett, T.S., Personal communication, 1999.

Dallimore, S.R., T. Uchida, and T.S. Collett (eds.), *Scientific Results from JAPEX/JNOC/GSC Mallik 2L-38 Gas Hydrate Research Well, Mackenzie Delta, Northwest Territories, Canada*, Geological Survey of Canada Bulletin 544, 1999.

Moridis, G.J., J. Apps, K. Pruess, and L. Myer, *EOSHYDR: A TOUGH2 Module for CH4-Hydrate Release and Flow In the Subsurface*, Report LBNL-42386, Lawrence Berkeley Laboratory, Berkeley, CA, 1998.

Moridis, G.J., *Numerical Studies of Gas Production from Methane Hydrates*, paper SPE 75691 presented at the 2002 SPE Gas Technology Symposium, Calgary, Alberta, Canada, April 30–May 2 (also Report LBNL-49765, Lawrence Berkeley National Laboratory, Berkeley, CA), 2002a.

Moridis, G.J., *Numerical Simulation Studies of Thermally-Induced Gas Production From Hydrate Accumulations With No Free Gas Zones at the Mallik Site, Mackenzie Delta, Canada*, paper SPE 77861 presented at the SPE Asia Pacific Oil and Gas Conference and Exhibition held in Melbourne, Australia, 8–10 October 2002 (also Report LBNL-50256, Lawrence Berkeley National Laboratory, Berkeley, CA), 2002b.

Moridis, G.J., T.S. Collett, S.R. Dallimore, T. Satoh, S. Hancock, and B. Weatherhill, *Numerical Studies of Gas Production Scenarios From Several CH_4-Hydrate Accumulations at the Mallik Site, Mackenzie Delta, Canada*, Report LBNL-50257, Lawrence Berkeley National Laboratory, Berkeley, CA, 2002.

Pruess, K., C. Oldenburg, and G. Moridis, *TOUGH2 User's Guide, Version 2.0*, Report LBNL-43134, Lawrence Berkeley National Laboratory, Berkeley, Calif., 1999.

Sloan, E.D.: *Clathrate Hydrates of Natural Gases*, Marcel Dekker, Inc., New York, NY, 1998.